Rapid solidification under local nonequilibrium conditions

S. L. Sobolev*
Institute of Chemical Physics, Academy of Sciences of Russia, Chernogolovka, Moscow Region, 142432 Russia
(Received 22 April 1996)

The effects of local nonequilibrium solute diffusion on a solute concentration field, solute partitioning, interface temperature, and absolute stability limit have been considered. The model incorporates two diffusive speeds, V_{Db}, the bulk-liquid diffusive speed, and V_{Di}, the interface diffusive speed, as the most important parameters governing the solute concentration in the liquid phase and solute partitioning. The analysis of the model predicts a transition from diffusion-controlled solidification to purely thermally controlled regimes, which occurs abruptly when the interface velocity V equals the bulk liquid diffusive speed V_{Db}. The abrupt change in the solidification mechanism is described by the velocity-dependent effective diffusion coefficient $D^*=D(1-V^2/V_{Db}^2)$ and the generalized partition coefficient K^*. If $V>V_{Db}$, then $D^*=0$ and $K^*=1$. This implies an undistributed diffusion field in the liquid (diffusionless solidification) and complete solute trapping at $V>V_{Db}$. [S1063-651X(97)08504-8]

PACS number(s): 66.10.−x, 81.30.Fb, 05.70.Ln

I. INTRODUCTION

Rapid phase transformation is a field of condensed-matter physics and materials science that has developed rapidly over the last years. It has proved to be of considerable interest for both applied and fundamental research for a variety of reasons discussed extensively in the literature [1–22]. During pulsed-laser annealing or rapid solidification of highly undercooled melts, the phase transformation occurs under conditions far from local equilibrium. The local nonequilibrium nature of this process has made it possible to study new crystal-growth mechanisms and amorphous solid formation kinetics, and produce metastable materials whose composition or structure is unobtainable by other methods. The deviations from local equilibrium affect not only the partitioning of species across the interface, but also the diffusion-temperature fields around the interface and the kinetics of crystal growth, which, in turn, influence the solidification mechanism [12,13].

The classical theoretical treatments of rapid solidification [1,2,6,17] take into account only the deviation from chemical equilibrium at the interface introducing the velocity-dependent partition coefficient. However, all aspects of the models assume local equilibrium in the liquid phase, and rely on the classical Fick law for the mass flux, which describes the spatial variation of the concentration field ahead of the interface as a continuous, smooth function. Such a modeling is valid only for relatively low interface velocities $V \ll V_{Db}$, where V_{Db} is the diffusive speed, i.e., the speed of propagation of diffusive disturbances [11–13,23–28]. With increasing undercooling—and correspondingly increasing driving force for crystallization—the growth rates increase, and may reach rates of the order of 100 m/s, while the diffusive speed is of the order of 1–10 m/s [1–5,9,22]. In these cases, i.e., when $V \sim V_{Db}$, the diffusion field in the liquid is far from local equilibrium, and the solute concentration and solute flux differ significantly from those predicted by the classical local equilibrium theory [12,13,23]. Our purpose is to provide: (1) a theoretical framework within which a hierarchy of deviations from equilibrium can be described; (2) a conceptual foundation, and a mathematical model based on it, for the study of local nonequilibrium solute transport associated with rapid solidification conditions; (3) analysis of the partitioning of species across the interface under the local-nonequilibrium conditions; and (4) analysis of the influence of the local nonequilibrium on the temperature field around the solid-liquid interface.

II. HIERARCHY OF DEVIATIONS FROM EQUILIBRIUM

In many situations, primarily those involving extremely short times or high propagation velocities, the mode of heat and/or mass transport is not diffusive (parabolic), but propagative (hyperbolic) [11–13,23–28]. The general theory of a fast-moving phase boundary [23] shows that the local nonequilibrium effects begin to play the most important role when the interface velocity V is of the order of the speed of signal (disturbance) propagation, i.e., the diffusive speed V_{Db} for mass (solute) transport or the speed of heat wave V_T for heat transport. If the interface velocity V is much less than the speeds of signals propagation, the corresponding fields (i.e., the solute concentration field for $V \ll V_{Db}$ or the temperature field for $V \ll V_T$) are in local equilibrium, and they can be described by the classical transport equation of parabolic type. If V is of the order of V_{Db}, the diffusion field is far from local equilibrium. If $V \sim V_T$, the temperature field is far from local equilibrium. In such situation the classical transport equation of parabolic type is no longer valid, and the local nonequilibrium effects should be taken into account [11–13,23–28].

The diffusive speed V_{Db} is of the order of 1–10 m/s, and the speed of the heat wave V_T is of the order of 10^3 m/s [1–6], i.e., $V_{Db} \ll V_T$. This implies that, as the interface velocity increases, the diffusional local equilibrium first breaks down at $V \sim V_{Db}$ and, after that, the thermal local equilibrium breaks down at $V \sim V_T$. This allows us to introduce a hierarchy of deviations from equilibrium which is followed with

*Electronic address: sobolev@icp.ac.ru

increasing solidification velocity:

(1) $V=0$. *Full equilibrium.* No chemical potential gradient (composition of phases are uniform), and no temperature gradients [10].

(2) $V \ll V_{\mathrm{Db}}$. *Local equilibrium.* There are concentration and temperature gradients near the interface; i.e., there is no full equilibrium, but there is local equilibrium both in the bulk liquid and at the interface. The partition coefficient is equal to its equilibrium value K_E. Certain hierarchies also exist within the case 2 [10].

(3) $V<V_{\mathrm{Db}}$. *Diffusional local equilibrium*. There is no local equilibrium at the interface, and the partition coefficient depends on the interface velocity V [1,2,6]. The solute concentration field is still in local equilibrium.

In cases (2) and (3), the solute concentration and temperature fields are governed by the classical (local equilibrium) transport equation of parabolic type.

(4) $V \sim V_{\mathrm{Db}}$. *Diffusional local nonequilibrium.* In this case solute diffusion occurs under local nonequilibrium conditions, and the solute concentration field is governed by the mass transport equation of hyperbolic type [11–13,23–27]. The temperature field is still at local equilibrium due to $V \sim V_{\mathrm{Db}} \ll V_T$, and it can still be described by the classical heat conduction equation of parabolic type.

(5) $V \sim V_T$. *Both diffusional and thermal local nonequilibrium.* At such high velocities there is no local equilibrium both for diffusion and heat transport processes. The solute concentration and temperature fields are governed by hyperbolic transport equations [23–27].

In this paper we consider in detail case (4) of deviations from local diffusional equilibrium. The case is of great practical interest [1,2], but it has received little attention in the literature [11–13].

III. LOCAL NONEQUILIBRIUM DIFFUSION FIELD

According to extended irreversible thermodynamics (EIT) [24–26], the simplest generalization of the classical Fick law for mass transport, which includes the relaxation to local equilibrium of the diffusion field, is given as

$$\mathbf{J}+\tau \partial \mathbf{J}/\partial t=-D\boldsymbol{\nabla} C \tag{1}$$

where $\mathbf{J}$ is the solute flux, C is the solute concentration, D is the diffusion coefficient, τ is the relaxation time of $\mathbf{J}$. In contrast to the Fick law, which leads to the diffusion equation of parabolic type, the evolutional equation (1) gives rise to the hyperbolic equations for the solute concentration and solute flux:

$$\frac{\partial C}{\partial t}+\frac{D\partial^2 C}{V_{\mathrm{Db}}^2 \partial t^2}=D\nabla^2 C, \tag{2}$$

$$\frac{\partial \mathbf{J}}{\partial t}+\frac{D\partial^2 \mathbf{J}}{V_{\mathrm{Db}}^2 \partial t^2}=D\boldsymbol{\nabla}(\boldsymbol{\nabla}\mathbf{J}). \tag{3}$$

The hyperbolic equations (2) and (3) predict the finite speed of the diffusive wave, i.e., the maximum speed with which the diffusional perturbations can propagate in the liquid [11–13,23–27]

$$V_{\mathrm{Db}}=(D/\tau)^{1/2}. \tag{4}$$

It should be noted that V_{Db} limits only the speed of perturbations, but the interface velocity V can be greater than V_{Db}. To derive the interface condition, we integrate the balance low over an infinitesimal zone that includes the interface between liquid and solid phases. The interface condition is

$$V(C-C_s)=J-J_s,$$

where C_s and J_s are the solute concentration and solute flux in the solid at the interface. Assuming $J_s=0$, and using Eq. (1), we can rewrite the interface condition as

$$(V+\tau\dot{V})(C-C_s)+\tau V\left(\frac{\partial C}{\partial t}-\frac{\partial C_s}{\partial t}\right)=-D\boldsymbol{\nabla} C, \tag{5}$$

where the superscript dot implies differentiation with respect to time. Note that condition (5) includes not only the interface velocity, but also the interface acceleration.

Now let us consider the solute concentration and solute flux fields ahead of the interface moving with constant average velocity $V=\mathrm{const}$. Following the usual steady-state approach, we view the solidification from a reference frame attached to a planar liquid-solid interface. In such a case, one-dimensional versions of Eqs. (2), (3), and (5) take the forms

$$D(1-V^2/V_{\mathrm{Db}}^2)\frac{d^2C}{dX^2}+V\frac{dC}{dX}=0, \tag{6}$$

$$D(1-V^2/V_{\mathrm{Db}}^2)\frac{dJ}{dX}+VJ=0, \tag{7}$$

$$V(C-C_s)=-D(1-V^2/V_{\mathrm{Db}}^2)\frac{dC}{dX}. \tag{8}$$

Equations (6) and (7) result in the solute concentration and solute flux distributions in the liquid $X>0$ (the origin of the reference frame is fixed on the interface $X=0$),

$$C(X)=\begin{cases}(C_i-C_0)\exp[-VX/D(1-V^2/V_{\mathrm{Db}}^2)]+C_0, \\ V<V_{\mathrm{Db}} \\ C_0, \quad V>V_{\mathrm{Db}},\end{cases} \tag{9}$$

$$J(X)=\begin{cases}J_i\exp[-VX/D(1-V^2/V_{\mathrm{Db}}^2)], \quad V<V_{\mathrm{Db}} \\ 0, \quad V>V_{\mathrm{Db}},\end{cases} \tag{9a}$$

where C_0 and C_i are the solute concentration in the liquid far from $(X\to\infty)$ and at the interface $(X=0)$, respectively, and J_i is the solute flux at the interface. The solute concentration and solute flux distributions (9) clearly demonstrate that the diffusion speed V_{Db} plays the most decisive role in rapid solidification. When $V<V_{\mathrm{Db}}$, the diffusion process affects the solute concentration field in the liquid, and the solidification is essentially controlled by the solute flux. It is noted that as the interface velocity approaches zero, the relaxational model approaches the classical formulation. However, as the velocity increases, the solute boundary layer

shrinks more rapidly than expected from the classical mass transport theory, and its thickness d defined as [see Eqs. (9)]

$$d(V/V_{\mathrm{Db}})=\begin{cases} D(1-V^2/V_{\mathrm{Db}}^2)/V, & V<V_{\mathrm{Db}} \\ 0, & V>V_{\mathrm{Db}} \end{cases} \tag{10}$$

approaches zero at $V=V_{\mathrm{Db}}$. The correct definition of characteristic lengths plays an important role in the analysis of the solidification microstructures [2]. When $V>V_{\mathrm{Db}}$, solutions (9) and (10) imply that the solute concentration and solute flux fields ahead of the interface are undisturbed. The result has a clear physical meaning: a source of perturbations (i.e., the interface) moving with a velocity greater than the maximum speed of perturbations cannot disturb the medium ahead of itself [12,13,23]. In this case, the solute atoms do not have enough velocity to escape the solid-liquid interface. Thus there is no diffusion of solute in the liquid at $V>V_{\mathrm{Db}}$ and, consequently, the solidification cannot be controlled by diffusion. Hence the solidification mechanism changes qualitatively when the interface velocity V passes through the critical point $V=V_{\mathrm{Db}}$. In this point, a sharp transition from diffusion controlled to purely thermally controlled growth occurs.

The behaviors of the solute concentration and solute flux distributions (9) and (10) allow us to introduce the effective diffusion coefficient D^* as [12,13]

$$D^*(V/V_{\mathrm{Db}})=\begin{cases} D(1-V^2/V_{\mathrm{Db}}^2), & V<V_{\mathrm{Db}} \\ 0, & V>V_{\mathrm{Db}}. \end{cases} \tag{11}$$

If $V\ll V_{\mathrm{Db}}$, the effective diffusion coefficient D^* reduces to the classical diffusion coefficient D for the local equilibrium conditions. But when V is of the order of V_{Db}, D^* predicts less solute flux $\mathbf{J}=-D^*\boldsymbol{\nabla}C$ than expected from the classical Fick law $\mathbf{J}=-D\boldsymbol{\nabla}C$. If $V\geqslant V_{\mathrm{Db}}$, then $D^*=0$. It implies the absence of solute diffusion ahead of the interface. Thus the local nonequilibrium effects in the bulk liquid lead to the diffusionless solidification, i.e., solidification with zero effective diffusion coefficient D^* [Eq. (11)], which can be reached at finite interface velocities $V\geqslant V_{\mathrm{Db}}$.

IV. PARTITION COEFFICIENT

The effective diffusion coefficient D^* can be used to modify some results of the local equilibrium theory by substituting D^* for D. For example, according to the continuous growth model (CGM) of Aziz and Kaplan [6], the partition coefficient $K(V)$ takes the form

$$K(V)=[K_E+V/V_{\mathrm{Di}}][1+V/V_{\mathrm{Di}}]^{-1},$$

where K_E is the equilibrium partition coefficient, and V_{Di} is a parameter for solute redistribution. The diffusive speed of our local nonequilibrium model, V_{Db}, and the parameter for solute redistribution of the CGM, V_{Di}, require further discussion. The CGM defines V_{Di} as the ratio of solute diffusivity *through the interface* D_i to the atomic jump distance *at the interface* λ_i [6,17]. In other words, V_{Di} is the average diffusive speed over the interface region, and it can be called *the interface diffusive speed* V_{Di} [17]. The interface diffusive speed is a kinetic rate parameter for solute redistribution at a relatively low interface velocity $V<V_{\mathrm{Db}}$. The local nonequilibrium model of solute transport, Eqs. (1)–(4), defines the diffusive speed V_{Db} as the speed of propagation of diffusive wave in the bulk liquid (see also Refs. [12,13,23–27]). Taking into account that the relaxation time τ in Eqs. (1), (4), and (5) can be rewritten as $\tau=\lambda/V_{\mathrm{Db}}$, where λ is the atomic jump distance *in the bulk liquid*, the diffusive speed in the local nonequilibrium solute diffusion model, Eqs. (2)–(4), takes the form

$$V_{\mathrm{Db}}=D/\lambda,$$

where D is the solute diffusion coefficient *in the bulk liquid*. Thus V_{Db} can be called *the bulk (liquid) diffusive speed*, i.e., the speed with which the solute atoms can diffuse in the bulk liquid. Assuming that $D_i\approx D$ and $\lambda_i\approx\lambda$, one is led to $V_{\mathrm{Di}}=V_{\mathrm{Db}}$. This assumption is a zeroth-order approximation, and it was considered in [12]. In a general case these two velocities can be different, and the partitioning of solute depends on both V_{Db} and V_{Di} [13].

Thus introduction of D^*, Eq. (11), into the expression for $K(V)$ leads to the generalized partition coefficient K^*,

$$K^*(V)=\begin{cases} \dfrac{K_E(1-V^2/V_{\mathrm{Db}}^2)+V/V_{\mathrm{Di}}}{(1-V^2/V_{\mathrm{Db}}^2)+V/V_{\mathrm{Di}}}, & V<V_{\mathrm{Db}} \\ 1, & V>V_{\mathrm{Db}}. \end{cases} \tag{12}$$

The local nonequilibrium partition coefficient K^*, Eq. (12), together with the prediction of CGM, are shown in Fig. 1 as functions of interface velocity V scaled to the bulk-liquid diffusive velocity V_{Db} with $V_{\mathrm{Db}}/V_{\mathrm{Di}}=2$. The choice of ratio between V_{Db} and V_{Di} will be discussed below. Expression (12) clearly demonstrates that the transition to complete the solute trapping $K^*=1$ occurs at a finite interface velocity

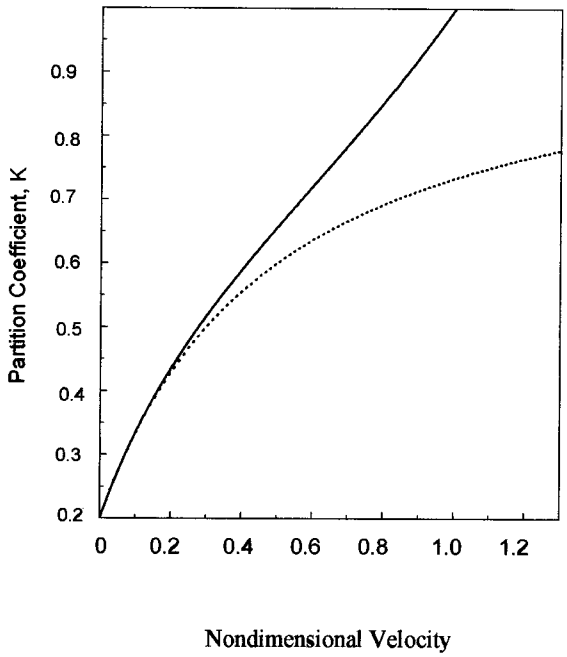

FIG. 1. Partition coefficient K as a function of interface velocity V scaled to the bulk liquid diffusive speed V_{Db}. Solid curve: the local-nonequilibrium model, Eq. (12); dotted curve: CGM.

$V = V_{Db}$, while the CGM predicts complete solute trapping only at $V \to \infty$ (see Fig. 1). The solute partitioning is governed by both the *interface* diffusive speed V_{Di} and the *bulk-liquid* diffusive speed V_{Db}. At a relatively low interface velocity $V \sim V_{Di} < V_{Db}$, the limiting stage for solute redistribution is the solute diffusion through the interface, and the solute partitioning is governed by V_{Di}. As the interface velocity increases, the diffusive coefficient D^*, Eq. (11), tends to zero, and the solute diffusion near the interface becomes a limiting stage for solute partitioning. In this case, the solute redistribution at the interface is governed by the bulk-liquid diffusive speed V_{Db}.

V. INTERFACE STABILITY

It is known that mass transport can lead to an instability of the solid-liquid interface [1,2,15,16,21]. Solute rejected by the interface creates a concentration gradient in the liquid layer next to the interface. The concentration gradient causes the liquid ahead of the interface to be undercooled. According to the interface stability theory (see Refs. [1,2,15,16,21] and references therein), the destabilizing effect of the concentration gradient is compensated by the stabilizing effect due to the interface energy (Gibbs-Thomson effect). From this theory a planar interface is stable for an alloy if the interface velocity V exceeds the absolute stability limit, V_a. Preliminary results [16,17,21] indicate that the classical absolute stability limit obtained by Mullins and Sekerka for the local equilibrium conditions [15] holds with velocity dependent $K(V)$ and $m(V)$. It allows us to assume (as a zeroth order approximation) that the local nonequilibrium stability limit can be obtained from the classical one [15] by replacing the local equilibrium K_E, m, and D with velocity dependent, local nonequilibrium $K^*(V)$, $m(V)$, and $D^*(V)$. Thus, for high velocities, the absolute stability limit with allowance for the local nonequilibrium effects takes the form

$$C_0 = \frac{[K^*(V_a)]^2 T_m \Gamma V_a}{m(V_a) D^*(V_a)[1 - K^*(V_a)]}; \tag{13}$$

here T_m is the melting point of pure solvent and Γ is the Gibbs-Thomson coefficient. Figure 2 shows the critical bulk concentration C_0 as a function of the nondimensional velocity V_a/V_{Db} calculated from Eq. (13). For the dotted curve, we used $K(V)$ from the CGM, and $D = \text{const}$. For the solid curve, the local nonequilibrium partition coefficient $K^*(V)$, Eq. (12), and the velocity dependent diffusion coefficient $D^*(V)$, Eq. (11), are used. Values for the thermophysical parameters corresponding to Si-Sn alloys are taken from [21]. For the sake of simplicity, we also assumed that m is equal to its equilibrium value in both cases due to relatively weak dependence of m on V. The value for V_a is very sensitive to local nonequilibrium effects because of the strong dependence of K^* and especially D^* on the interface velocity. These effects stabilize the interface due to the decreasing solute diffusion at $V \to V_{Db}$ [see Eq. (11)]. If $V > V_{Db}$, there is no solute gradient ahead of the interface and, therefore, there are no destabilizing effects. This implies that the planar interface is stable at $V > V_{Db}$, and the limit of absolute stability V_a is smaller than V_{Db} at any values for C_0 and other parameters (see Fig. 2). Expression (13) can be rearranged in the form

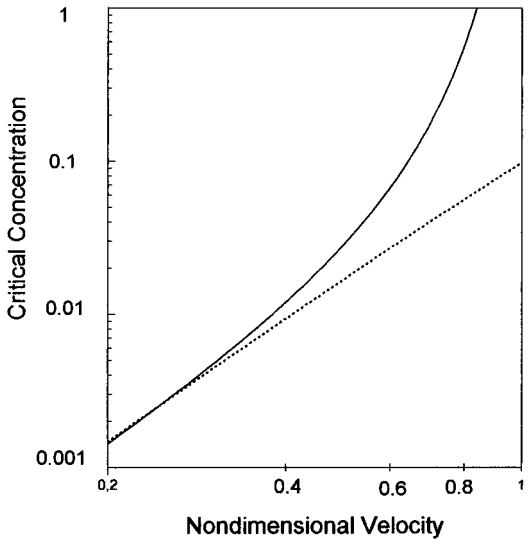

FIG. 2. Critical concentration as a function of the velocity of absolute stability limit V_a scales to V_{Db}. Solid curve: Eq. (13) assuming local nonequilibrium in the bulk liquid with $D(V)$ and $K(V)$ given by Eqs. (11) and (12). Dotted curve: Eq. (13) assuming local equilibrium in the bulk liquid with $D = \text{const}$ and $K(V)$ given by the CGM.

$$V_a = V_{ae}(1 - V_a^2/V_{Db}^2),$$

where V_{ae} is the classical absolute stability limit [15], with $K(V)$ predicted by the CGM (dotted curve in Fig. 2). The solution to the last equation, to leading order in small parameter V_{ae}/V_{Db}, results in

$$V_a = V_{ae}(1 - V_{ae}^2/4V_{Db}^2).$$

This implies that the absolute stability limit with allowance for the local nonequilibrium effects V_a (the solid curve in Fig. 2) is smaller than V_{ae} (the dotted curve in Fig. 2) at the same value for C_0. Thus the local nonequilibrium effects stabilize the interface, and reduce the value for V_a due to the decreasing solute diffusion.

A more general solution to the interface stability problem should be based on the analysis of the hyperbolic mass transport equation (2). In a moving reference frame, a one-dimensional version of Eq. (2) takes the form

$$\partial C/\partial t - V \partial C/\partial X + D V_{Db}^{-2} \partial^2 C/\partial t^2 = D(1 - V^2/V_{Db}^2)\partial^2 C/\partial X^2.$$

Now we take the Fourier transform of this equation in both time and space ($\partial/\partial t \leftrightarrow i\omega$, $\partial/\partial X \leftrightarrow ih$) to obtain the dispersion law

$$\omega - V h_1 = -2D(1 - V^2/V_{Db}^2) h_1 h_2,$$

$$V h_1^2 - D\omega^2/V_{Db}^2 = -D(1 - V^2/V_{Db}^2)(h_1^2 - h_2^2),$$

where h_1 and h_2 are real, and $h=h_1+ih_2$. These equations can be solved for the wave number $h_1(\omega)$ and attenuation $h_2(\omega)$, but such expressions are rather awkward. Here we are interested only in the asymptotical behavior of the wave number $h_1(\omega)$. If $V \ll V_{\rm Db}$, the spectrum is purely diffusive with $h_1^2 \sim \omega$. As the velocity V increases (but $V<V_{\rm Db}$), the spectrum transforms to the wave spectrum $h_1^2 \sim \omega^2$. In this case, numerical simulations reveal an increase of the amplitude of the perturbations at the wave front [27]. Such an increase of the concentrational oscillations is to be expected at the solid-liquid interface under rapid solidification conditions. However, if $V>V_{\rm Db}$, $D^*=0$, and the solidification front cannot disturb the concentration field in the liquid. Hence, when V passes through the critical point $V=V_{\rm Db}$, a sharp drop of the amplitude of the diffusional oscillations at the interface is expected. These oscillations affect the structure of the solidified phase [1,2], and may also play an important role in grain refinement, which occurs at $V=V_{\rm Db}$ [1], but the problem requires special consideration.

VI. INTERFACE TEMPERATURE

We now consider the influence of the local-nonequilibrium solute diffusion on the interface temperature. This will be done by including the velocity-dependent diffusion coefficient (11) and the generalized partition coefficient (12) obtained in Sec. IV into the results of the dendritic growth theory for a plane interface and an Ivantsov dendrite (see Refs. [1,2], and references therein).

A. Planar front growth

The planar front temperature under steady-state growth can be written as [2]

$$T_i = T_s + \left(\frac{m(V)}{K(V)} - \frac{m}{K_E} \right) C_0 - \frac{V}{\mu}, \tag{14}$$

where T_i is the interface temperature, T_s is the equilibrium solidus temperature of the alloy, μ is the interface kinetic coefficient, and $m(V)$ is the effective liquidus slope. The physical interpretation of $m(V)$ is that it represents the slope of the line in the phase diagram that connects the melting point of pure solvent with the nonequilibrium interface composition in the liquid at a given interface temperature in the absence of interface attachment kinetic effects [2]. The effective liquidus slope $m(V)$ is given by [1,2,10]

$$m(V) = m \left(\frac{1 - K(V) + K(V) \ln(K(V)/K_E)}{1 - K_E} \right).$$

Under local equilibrium conditions, the planar interface temperature is T_s, but, as the local nonequilibrium effects become important, the planar interface temperature increases because of the increase in the effective solidus temperature, and their increase is represented by the second term in Eq. (14). If $V \to V_{\rm Db}$, then $K(V) \to 1$, and the effective solidus temperature

$$T_s^* = T_s + \left(\frac{m(V)}{K(V)} - \frac{m}{K_E} \right) C_0 \tag{15}$$

reaches its maximum value

$$T_{s\max}^* = T_s + \left(\frac{K_E - 1 - K_E \ln K_E}{K_E(1-K_E)} \right) m C_0. \tag{16}$$

When $V>V_{\rm Db}$, the effective solidus temperature T_s^*, Eq. (14), does not depend on the interface velocity V, and is equal to its maximum value $T_{s\max}^* = T_0$. Thus the effective solidus temperature T_s^* changes from the equilibrium solidus temperature T_s at $V=0$ to its maximum value $T_{s\max}^* = T_0$ at $V=V_{\rm Db}$.

If $V>V_{\rm Db}$, then Eqs. (14)–(16) imply that the planar front temperature T_i decreases linearly with V at due to the interface attachment kinetics,

$$T_i = T_{s\max}^* - V/\mu. \tag{17}$$

Thus the variation of the steady-state planar interface temperature shows a maximum at $V \sim V_D$.

B. Rapid dendritic growth

The basic dendrite growth model is given by the tip undercooling expression and the dendrite tip selection criterion (see Refs. [1,2,10], and references therein). To extend the model on the case of local nonequilibrium growth with $V \sim V_{\rm Db}$, we apply the result of Sec. III to the tip of an Ivantsov dendrite. The tip undercooling equation is given by

$$\Delta T(V) = \Delta T_t(V) + \Delta T_s(V) + \Delta T_R(V) + \Delta T_K(V) + \Delta T_{\rm ne}(V),$$

where ΔT_t, ΔT_s, ΔT_R, and ΔT_K are the thermal, solutal, curvature, and kinetic undercooling, respectively. An additional term

$$\Delta T_{\rm ne} = (m - m(V)) C_0 \tag{18}$$

arises due to the difference between the slope of the equilibrium phase diagram m and the slope of the nonequilibrium phase diagram $m(V)$ [2]. Substituting D^* for D and K^* for K in the expression for the solute undercooling [1,2], the local nonequilibrium solute undercooling takes the form

$$\Delta T_s^* = m(V) C_0 \left[1 - \frac{1}{1 - (1 - K^*(V)) \mathrm{Iv}(P_c^*)} \right]$$

where $\mathrm{Iv}(P_c^*)$ is the Ivantsov function in terms of the local nonequilibrium Peclet number $P_c^* = VR/2D^*$. Here D^* is the effective diffusion coefficient, Eq. (11), and R is the dendrite tip radius. If $V \to V_{\rm Db}$, then $D^* \to 0$, $P_c^* \to \infty$, $\mathrm{Iv} \to 1$, and $K^* \to 1$. This implies that the solutal undercooling $\Delta T_s^* = 0$ at $V>V_{\rm Db}$. The additional term $\Delta T_{\rm ne}$ reaches at $V=V_{\rm Db}$ its maximum value

$$\Delta T_{\rm ne}^{\max} = m C_0 \left(\frac{\ln K_E - K_E + 1}{1 - K_E} \right), \tag{19}$$

and does not change at $V>V_{\rm Db}$. Thus, when the interface velocity passes through the critical point $V=V_{\rm Db}$, the $\Delta T(V)$ relationship will drastically change. If $V<V_{\rm Db}$, the dendrites are mostly solute diffusion controlled, and the $\Delta T(V)$ curve is essentially dependent on $\Delta T_s^*(V)$ and

$\Delta T_{ne}(V)$. As the interface velocity increases, the deviations from local diffusional equilibrium will progressively arise, leading to a growing partition coefficient K^* and a decreasing effective diffusion coefficient $D^*(V)$. When $V>V_{Db}$, then $K^*=1$, $D^*=0$, $\Delta T_s^*=0$, and $T_{ne}=\Delta T_{ne}^{max}$. In such a case, the sample will solidify, and be diffusionless and partitionless, with the consequence that supersaturated solid solutions are formed. The interface undercooling does not depend on the solute diffusion, and is given as

$$\Delta T(V)=\Delta T_t(V)+\Delta T_R(V)+\Delta T_K(V)+\Delta T_{ne}^{max}.$$

Thus, a sharp transition from a mostly solutal to a purely thermal growth is expected at $V=V_{Db}$.

The general tip radius selection criterion in an undercooled alloy melt in the first approximation can be obtained from local equilibrium theory [1,2], except that $K(V)$ and D are again replaced by $K^*(V)$ and $D^*(V)$, respectively. The resulting equation for the tip radius reads

$$R=\frac{4\pi^2\Gamma}{\Theta_t P_t \xi_c+2\Theta_c P_c^* \xi_c},$$

where Γ is the Gibbs-Thomson coefficient, Θ is the hypercooling limit, and

$$\xi_t=1-\frac{1}{[1+(2\pi/P_t)^2]^{1/2}},$$

$$\xi_c=1+\frac{2K^*}{1-2K^*-[1+(2\pi/P_c^*)^2]^{1/2}},$$

$$\Theta_c=\frac{2mC_0(K^*-1)}{1-(1-K^*)\mathrm{Iv}(P_c^*)}.$$

As the interface velocity V increases, the stability function ξ_c begins to deviate from unity, and is equal to zero at $V=V_{Db}$. When $V>V_{Db}$, then $\xi_c=0$, and the dendrite tip radius R depends only on thermal and capillarity effects. Thus, when the interface velocity V passes through the critical point $V=V_{Db}$, the most important parameters of the dendrite growth will change drastically. Expressions for these parameters are summarized in Table I.

It should be noted that in this section we assume that the local nonequilibrium effects do not affect the shape of the solid-liquid interface, and the Ivantsov solution for a parabolic needle with a constant interface temperature and composition are still valid at $V\sim V_{Db}$. Strictly speaking, the shape of the interface depends on the deviation from local equilibrium due to the velocity-dependent effective diffusion coefficient $D^*(V)$ and velocity-dependent partition coefficient $K^*(V)$. The precise shape preserving (invariant) solution of the steady-state dendrite growth under the local nonequilibrium condition must be determined such that the solutions of the heat conduction equation of parabolic type and the solute transport equation of hyperbolic type (2) satisfy the shape-preserving conditions. This conditions should also take into account the lower value of the normal velocity V_n and, hence, the lower value of $K^*(V_n)$ along the sides of the dendrite tip [5].

TABLE I. Important parameters of dendritic growth at $V<V_{Db}$ and $V>V_{Db}$.

$V<V_{Db}$	$V\geqslant V_{Db}$
$D^*=D(1-V^2/V_{Db}^2)$	0
$d=D(1-V^2/V_{Db}^2)/V$	0
$K^*=\dfrac{K_E(1-V^2/V_{Db}^2)+V/V_{Di}}{(1-V^2/V_{Db}^2)+V/V_{Di}}$	1
$P_C^*=VR/2D(1-V^2/V_{Db}^2)$	∞
$\mathrm{Iv}(P_C^*)$	1
$C_i^*=C_0/[1-(1-K^*)\mathrm{Iv}(P_C^*)]$	C_0
$\Delta T_S^*=m(V)C_0[1-(1-(1-K^*)\mathrm{Iv}(P_C^*))^{-1}]$	0
$\zeta_C=1+\dfrac{2K^*}{1-2K^*-[1+(2\pi/P_C^*)^2]^{1/2}}$	0
$R=\dfrac{4\pi^2\Gamma}{\theta_i P_t\zeta_t+2\theta_C P_C\zeta_C}$	$\dfrac{4\pi^2\Gamma}{\theta_t P_t\zeta_t}$

VII. ON THE KINETICS OF LOCAL NONEQUILIBRIUM CRYSTAL GROWTH

In modeling the velocity-undercooling function for solidification of alloys, the growth velocity is typically expressed as

$$V(T)=V_0(1-\exp(-\Delta G/RT)),$$

where ΔG is the Gibbs free-energy change per mole of material solidified, V_0 is the kinetic prefactor, and R is the gas constant. The driving force for solidification, ΔG, depends on the chemical potential changes of solvent and solute at the interface, which are usually calculated on the basis of classical, local equilibrium thermodynamics. According to EIT [24–26], the generalized Gibbs equation and entropy production equation have the forms

$$dS=dS_{eq}-\beta\tau\mathbf{J}\cdot\mathbf{J} \tag{20a}$$

$$\sigma=\sigma_{eq}-2\beta\tau\mathbf{J}\cdot d\mathbf{J}/dt \tag{20b}$$

where S_{eq} and σ_{eq} are the equilibrium entropy and entropy production, respectively, and β is the coefficient. The nonclassical terms in Eq. (20) play an important role when the system is far from local equilibrium. In a steady-state regime when the solid-liquid interface moves with a constant velocity V, a degree of deviation from local equilibrium depends on the ratio V/V_{Db}. Indeed, in a moving frame of reference, Eq. (20b) can be rewritten as

$$\sigma=\sigma_{eq}-2\beta DVV_D^{-2}\mathbf{J}\cdot d\mathbf{J}/dX.$$

Thus, in a steady-state regime with high velocity $V\sim V_{Db}$, the system is far from local equilibrium and the entropy, as

TABLE II. Hierarchy of deviations from equilibrium.

$V=0$	Global equilibrium	$T=\text{const},\ C=\text{const}$
$V \ll V_{\mathrm{Db}}$	Local equilibrium both in the bulk liquid and at the interface) $K=K_E\ \ d=D/V$	$J=-D\nabla C$ $q=-\lambda\nabla T$
$V<V_{\mathrm{Db}}$	Diffusional local equilibrium (no equilibrium at the interface) $K=K(V)\ \ d=D/V$	$\partial C/\partial t=D\nabla^2 C$ $\partial T/\partial t=a\nabla^2 T$
$V\sim V_{\mathrm{Db}}$	Diffusional local nonequilibrium (both in the bulk liquid and at the interface) $K=K^*\rightarrow 1$ $D^*=D(1-V^2/V_{\mathrm{Db}}^2)\rightarrow 0$ $d=D(1-V^2/V_{\mathrm{Db}}^2)/V\rightarrow 0$	$\mathbf{J}+\tau\partial\mathbf{J}/\partial t=-D\nabla C$ $\frac{\partial C}{\partial t}+\tau\frac{\partial^2 C}{\partial t^2}=D\nabla^2 C$
$V>V_{\mathrm{Db}}$	$K^*=1\ \ D^*=0\ \ d=0$	$C=C_0=\text{const}\ \ J=0$
$V\sim V_T$	Diffusional and thermal local nonequilibrium	$(\partial T/\partial t)+\tau_T(\partial^2 T/\partial t^2)=a\nabla^2 T$ $\mathbf{q}+\tau_T\partial\mathbf{q}/\partial t=-\lambda\nabla T$

well as the other thermodynamic functions, is velocity dependent. In such a case, the Gibbs free-energy change ΔG takes the form

$$\Delta G=\Delta G_{\mathrm{eq}}+\Delta G(V).$$

$\Delta G(V)$ may be complicated functions of V, but they must go to zero as $V\rightarrow 0$, and must increase as $V\rightarrow V_{\mathrm{Db}}$. The expression for $\Delta G(V)$ can be obtained in the framework of EIT [24]–[26], and it is planned to be reported in future papers.

VIII. DISCUSSION

In the previous sections we presented and analyzed a local-nonequilibrium model of solute transport under rapid solidification conditions. In particular the solution to this model in the steady-state regimes $V=\text{const}$ has been considered. The most important difference between the present model and its predecessors is the incorporation of three characteristic velocity scales: i.e., the interface diffusive speed V_{Di}, the bulk-liquid diffusive speed V_{Di}, and the speed of heat wave V_T into the heat-mass transport problem. These velocity scales define different degrees of deviation from equilibrium during solidification. Different degrees of nonequilibrium imply different solidification regimes, which should be described by heat-mass transport equations of parabolic or hyperbolic type (see Table II).

Our results clearly demonstrate that the solidification mechanism changes qualitatively when the interface velocity V passes through the critical point $V=V_{\mathrm{Db}}$. At this point a sharp transition from mostly diffusion-controlled to purely thermally controlled regimes occurs. When $V<V_{\mathrm{Db}}$, there is a solute concentration gradient near the interface, and the solidification is governed by both redistribution of heat and solute, whereas at $V>V_{\mathrm{Db}}$ there is no solute concentration gradient in the bulk liquid, and solidification is purely thermally controlled with zero effective solute diffusion coefficient $[D^*(V)=0]$. It is predicted from thermodynamic arguments that the liquidus and solidus lines approach the T_0 curve, which is the thermodynamic limit to diffusionless solidification, at infinite growth velocity [20]. According to our model, the T_0 curve and diffusionless solidification can be reached at a finite interface velocity $V=V_{\mathrm{Db}}$. Walder and Ryder [7] showed that a sharp transition from diffusion-controlled to purely thermally controlled growth for Ag-Cu alloys corresponds to T_0 temperature, and occurs at finite interface velocity. The same results have been obtained by Walder for Ti-Ni alloys [8]. Such a sharp transition from diffusion-controlled to purely thermally controlled growth was also observed in Cu-Ni alloys [3] and Ni-B alloys [4] under rapid solidification conditions (see also Refs. [1,5]). The investigations [3,4] showed that it is not a critical undercooling that initiates the transition, but rather a critical solidification velocity, which approximately equals the diffusive speed. Thus the experimental results [3–8] give strong support to the idea that the local nonequilibrium solute transport and the bulk-liquid diffusive speed described here play an important role in rapid solidification, and govern the transition to diffusionless solidification, which occurs at a finite interface velocity $V=V_{\mathrm{Db}}$.

The transition to diffusionless solidification is accompanied by complete solute trapping $K^*(V)=1$. The complete solute trapping at a finite interface velocity has also been observed in experimental measurements. For example, values for $K=1$ have been determined for B, P, and As impurities in silicon at growth velocities of 2.7–4.5 m/s which can be achieved by pulsed-laser annealing [20,21]. A molecular-dynamics study by Cook and Clancy [18] for a Lennard-Jones system also showed complete solute trapping for unstrained growth on (100) when the interface velocity attained its steady-state regrowth value of 4 m/s. The CGM fails to predict the complete solute trapping observed in the simula-

TABLE III. Values for the ratio $g(n)=D_i/D$ between the average interface diffusion coefficient D_i and the bulk-liquid diffusion coefficient D for the diffusive interface consisting of n solid-liquid interfacial planes.

n	1	2	3	4	5
$g(n)$	0.5	0.37	0.33	0.29	0.26

tion [18]. In this case $V \geqslant V_{\mathrm{Db}}$, and, according to Eq. (12), our model predicts $K=1$, which is in agreement with the molecular-dynamics study.

The interface region between pure solid and pure liquid phases can be treated as a two-phase zone consisting of both phases. This implies that the interface diffusive coefficient D_i attains a value between D, the bulk liquid diffusion coefficient, and $D_s \approx 0$, the bulk solid diffusion coefficient. For example, a nonequilibrium molecular-dynamics simulation [18] indicated that the interface diffusion coefficient can be as much as 5–10 times less than in the bulk liquid. This also holds true for the interface diffusive speed, i.e., $V_{\mathrm{Db}} > V_{\mathrm{Di}} > V_{\mathrm{Ds}} \approx 0$, where V_{Ds} is the diffusive speed in the solid. For an atomically abrupt solid-liquid interface consisting of one solid-liquid interfacial plane, it is reasonable to assume that $V_{\mathrm{Di}}=(V_{\mathrm{Db}}+V_{\mathrm{DS}})/2 \approx V_{\mathrm{Db}}/2$. If we adopt this idea for the diffusive interface consisting of n solid-liquid interfacial planes, and use a value for the diffusive speed V_{Dk} in the kth atomic layer equal to half a sum of the diffusive speed of its nearest-neighbor layers, $V_{D(k+1)}$ and $V_{D(k-1)}$, the average interface diffusive speed V_{Di} and the average interface diffusion coefficient D_i take the form $V_{\mathrm{Di}}=g(n)V_{\mathrm{Db}}$ and $D_i=g(n)D$, where $g(n)$ is a coefficient. The values for $g(n)$ are given in Table III. For $n>6$ one can approximately estimate $g(n)$ as $1/n$. Thus the interface diffusive speed V_{Di} can be determined by dividing the interface diffusion coefficient D_i, which is an average diffusion coefficient over the interface region, by the atomic layer spacing λ, i.e., $V_{\mathrm{Di}}=D_i/\lambda=Dg(n)/\lambda$. On the other hand, it can be treated as a ratio between the bulk-liquid diffusion coefficient D and the effective interface width $L=\lambda/g(n)$.

The velocity dependence of the partition coefficient was measured for rapid solidification of polycrystalline Si-As alloys induced by pulsed-laser melting [9]. The experimental results are compared with predictions of the CGM and our local nonequilibrium model, Eq. (12), on Fig. 3. The CGM fits the data well only at a relatively low interface velocity with the diffusive speed of 0.46 m/s [9]. Our model fits the experimental results better at $V_{\mathrm{Di}}=0.75$ m/s and $V_{\mathrm{Db}}=2.7$ m/s (see Fig. 3).

The K vs V experimental data obtained by pulsed-laser melting of Ge-Si alloys [22] are shown in Fig. 4 together with the predictions of both CGM and Eq. (12). At a relatively low interface velocity, the CGM accurately fits the data at $K_E=0.4$ and $V_{\mathrm{Di}}=2$ m/s. Using the same K_E and V_{Di} results in a best-fit V_{Db} of 4.9 m/s at high interface velocities. Figure 4 shows that the local nonequilibrium model, Eq. (12), describes the data very well both at low and high interface velocities. Note that for Si-As alloys the interface diffusive speed V_{Di} is approximately one-fourth, and for

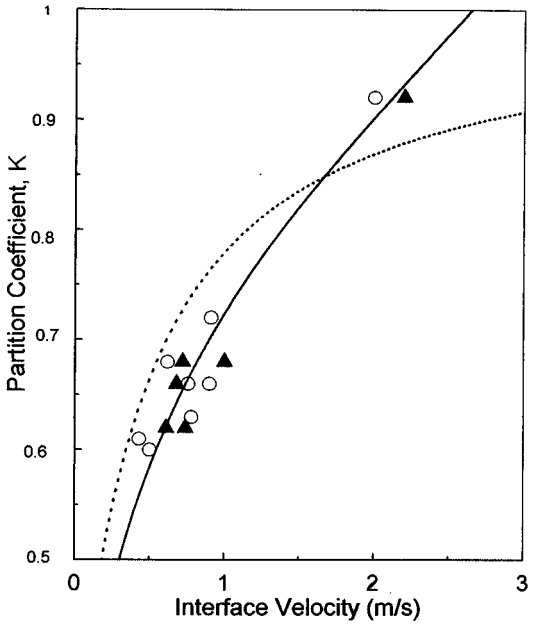

FIG. 3. Partition coefficient K as a function of interface velocity for Si-As alloys. Data points are from Ref. [9]; the dashed curve represents the Aziz model [6,17], with $K_E=0.3$ and $V_{\mathrm{Di}}=0.46$ m/s; the solid curve is obtained from Eq. (12) with the same K_E and $V_{\mathrm{Di}}=0.75$ m/s and $V_{\mathrm{Db}}=2.7$ m/s.

Ge-Si alloys is half as much as the bulk diffusive speed V_{Db}. This finding is consistent with our remark that the value of V_{Di} ranges between V_{Db} and $V_{\mathrm{DS}} \approx 0$. For Ge-Si alloys, Yu and Clancy [19] calculated a diffusive speed of 5 m/s, dividing the diffusion coefficient by the atomic layer

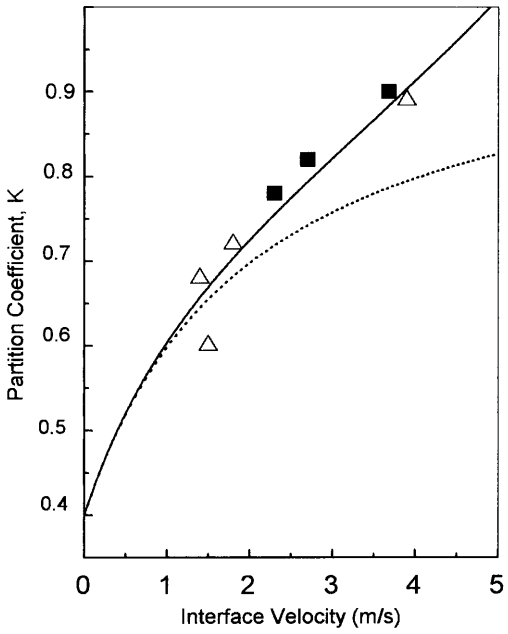

FIG. 4. Partition coefficient plotted vs interface velocity for Si-Ge alloys. Data points are from Ref. [22]; the dashed curve represents the Aziz model [6,17], with $K_E=0.4$ and $V_{\mathrm{Di}}=2$ m/s; the solid curve is obtained from Eq. (12) with the same K_E and V_{Di}; and $V_{\mathrm{Db}}=4.9$ m/s.

spacing. This value is very close to the fitted value for the bulk diffusive speed $V_{\mathrm{Db}}=4.9$ m/s obtained in our local nonequilibrium model (see Fig. 4). The relation between V_{Db} and V_{Di} corresponds to two atomic layers in our model (see Table III), and three atomic layer in Ref. [19]. Thus the local nonequilibrium results for the partition coefficient reproduced the experimental determination with good accuracy.

The results of an investigation of the solidification behavior of undercooled bulk Ag-Cu alloys were presented by Walder and Ryder [7]. It was shown that when the interface undercooling exceeded the T_0 temperature for all Ag-Cu alloys investigated, an abrupt increase of the growth rate was observed. At critical undercooling, the experimental values of Ag-Cu alloys approached those of pure Cu. In a recent paper, Walder observed the same critical behavior of the $V(\Delta T)$ curve in Ti-Ni alloys [8]. The sharp rise of the measured growth velocities at a critical undercooling was also observed for Ni-B alloys [4]. Note that the rise of the measured growth velocities is sharper than its theoretical prediction, especially for the Ni-1 at. % B sample [5]. This discrepancy was attributed to the model's assumption of smooth concentration profiles ahead of the solidification front [5]. The smooth concentration profiles arise due to the classical (i.e., local equilibrium) Fick law for mass flux. When $V=V_{\mathrm{Db}}$, our model predicts a discontinuous change in the diffusion field [see Eqs. (9) and (10)], and consequently a sharper rise of the growth velocity than expected from the classical theory.

To describe the sharp rise of the growth velocity, Walder and Ryder [7] proposed a simple empirical expression, which ensured that the liquidus and solidus lines approached the T_0 curve for infinite growth rates. If the expression is modified with the effective diffusion coefficient (11), the liquidus and solidus lines coincide for $V\geqslant V_{\mathrm{Db}}$ [8]. This simple empirical term is similar to the additional undercooling $\Delta T_{\mathrm{ne}}=T_s^*-T_s$ obtained here, taking into account the velocity-dependent slope of the phase diagram and the local nonequilibrium solute diffusion [see Eqs. (14)–(16), (18), and (19)]. Note that the calculated growth rate as a function of undercooling with the velocity-dependent diffusion coefficient $D^*(V)$, Eq. (11), fits the experimental data quite well, and exhibits a steeper rise at a critical undercooling than it is expected from classical consideration [8].

The experimental measurements of solidification velocities as a function of undercooling for Cu-Ni [3] alloys show that the transition from diffusion-controlled to thermally controlled growth is accompanied by a change of the $V(\Delta T)$ curve from a power law $V\sim\Delta T^{\beta}$ with $\beta\approx 3$ to a linear dependence $V\sim\Delta T$. The linear dependence differs markedly from current predictions [3]. According to our model, as the interface undercooling increases, the interface velocity first reaches the absolute stability limit V_a and then the diffusive speed V_{Db} because $V_a<V_{\mathrm{Db}}$. When the interface velocity passes through the point $V=V_a$, a transition from diffusive dendritic growth to thermal dendritic growth with almost planar interface occurs ($R_T\gg R$, due to $a\gg D$, where R_T and R are the dendrite tip radii of thermal and diffusive growth, respectively, and a is the thermal diffusivity). If $V>V_{\mathrm{Db}}$, then there are no solutal and curvature undercoolings at the interface (or curvature undercooling is very small due to $R_T\gg R$), and the interface velocity varies linearly with the total undercooling, i.e., $V\sim\Delta T$ at $V>V_{\mathrm{Db}}$ (see Sec. V A). Thus the linear dependence $V\sim\Delta T$ observed in the experiments [3] may correspond to a planar interface (or almost planar with $R_T\gg R$) growth without solutal undercooling due to diffusionless solidification $D^*(V)=0$ at $V>V_{\mathrm{Db}}$.

IX. CONCLUSION

(1) During rapid solidification different degrees of nonequilibrium constitute a hierarchy which is followed with increasing solidification velocity: (i) full equilibrium, (ii) local equilibrium, (iii) local interface nonequilibrium, (iv) diffusional local nonequilibrium, and (v) thermal local nonequilibrium.

(2) The effects of deviations from local equilibrium on solute concentration field can be described by the velocity-dependent diffusion coefficient $D^*(V)$, Eq. (11). If $V>V_{\mathrm{Db}}$, where V_{Db} is the *bulk-liquid diffusive speed*, then the solid-liquid interface does not disturb the solute concentration field in the liquid, and the effective diffusion coefficient $D^*(V)$ is equal to zero. These imply a transition to diffusionless solidification when the interface velocity V passes through the critical point $V=V_{\mathrm{Db}}$.

(3) The transition to diffusionless solidification is accompanied by complete solute trapping with $K^*\equiv 1$ at $V>V_{\mathrm{Db}}$. The solute partitioning is governed by two kinetic rate parameters: the *interface* diffusive speed V_{Di} and the *bulk-liquid* diffusive speed V_{Db}. The bulk-liquid diffusive speed V_{Db} is the speed of propagation of diffusive disturbances in the bulk liquid, i.e., the speed with which the solute atoms can diffuse in the bulk liquid. The speed is equal to the ratio between the bulk-liquid diffusive coefficient and the jump distance in the liquid. The interface diffusive speed V_{Di} can be treated as an average velocity with which solute atoms diffuse through the interface. At a relatively low interface velocity $V\sim V_{\mathrm{Di}}<V_{\mathrm{Db}}$, the limiting stage for solute redistribution is the solute diffusion through the interface and the solute partitioning is governed by V_{Di}. As the interface velocity increases, the diffusive coefficient D^*, Eq. (11), tends to zero, and the solute diffusion near the interface becomes the limiting stage for solute partitioning. In this case, the solute redistribution at the interface is governed by the bulk liquid diffusive speed V_{Db}.

(4) When $V>V_{\mathrm{Db}}$, there is no solutal undercooling, and the additional term ΔT_{ne} due to the difference between the slope of the equilibrium and local nonequilibrium phase diagrams has its maximum value.

(5) The local-nonequilibrium effects play a stabilizing role at high interface velocities, and decrease the value of the velocity of the absolute stability V_a, which is always less than V_{Db}.

(6) The directional solidification with a planar interface at $V>V_{\mathrm{Db}}>V_a$ obeys the linear dependence $V\sim\Delta T$ due to the kinetic undercooling.

Finally, there are still many other aspects of the problem where the local-nonequilibrium effects should be taken into account. As future directions for the theoretical research the following subjects seem promising to the author: interface kinetics, interface stability, the shape-preserving condition for the dendrite tip, the selection criterion for dendrites, and models for banded structures and grain refinement phenomenon.

[1] D. M. Herlach, Mater. Sci. Eng. **R12**, 177 (1994).
[2] R. Trivedi and W. Kurz, Int. Mater. Rev. **39**, 49 (1994).
[3] R. Willnecker, D. M. Herlach, and B. Feuerbacher, Phys. Rev. Lett. **62**, 2709 (1989); Appl. Phys. Lett. **56**, 324 (1990).
[4] K. Eckler, R. F. Cochrane, D. M. Herlach, B. Feuerbacher, and M. Jurisch, Phys. Rev. B **45**, 5019 (1992).
[5] K. Eckler, D. M. Herlach, and M. J. Aziz, Acta Metall. Mater. **42**, 975 (1994).
[6] M. J. Aziz and T. Kaplan, Acta Metall. **36**, 2335 (1988).
[7] S. Walder and P. L. Ryder, J. Appl. Phys. **74**, 6100 (1993); Acta Metall. Mater. **43**, 4007 (1995); A **133**, 698 (1991).
[8] S. Walder (unpublished).
[9] J. A. Kittl, M. J. Aziz, D. P. Brunco, and M. O. Thompson, J. Cryst. Growth **148**, 172 (1995).
[10] W. J. Boettinger and S. R. Coriell, in *Science and Technology of the Undercooled Melt*, edited by P. R. Sham, H. Jones, and C. M. Adam (Nijhoff, Dordrecht, 1986), p. 81.
[11] P. Galenko, Phys. Lett. A **190**, 292 (1994).
[12] S. L. Sobolev, Phys. Lett. A **199**, 383 (1995).
[13] S. L. Sobolev, Phys. Status Solidi A **156**, 293 (1996).
[14] T. Kraft and H. E. Exner, Mater. Sci. Eng. A **173**, 149 (1993).
[15] W. W. Mullins and R. F. Sekerka, J. Appl. Phys. **35**, 444 (1964).
[16] G. J. Merchant and S. H. Davis, Acta Metall. Mater. **38**, 2683 (1990).
[17] M. J. Aziz, Mater. Sci. Eng. A **178**, 167 (1994).
[18] S. J. Cook and P. Clancy, J. Chem. Phys. **99**, 2175 (1993).
[19] Q. Yu and P. Clancy, J. Crys. Growth **149**, 45 (1995).
[20] C. W. White, in *Laser and Electron-Beam Interactions with Solid*, edited by B. R. Appleton and G. K. Celler (North-Holland, Amsterdam, 1982), p. 109.
[21] D. E. Hoglund and M. J. Aziz, in *Kinetics of Phase Transformations*, edited by M. O. Thompson, M. Aziz, and G. E. Stephenson, MRS Symposia Proceedings No. 205 (Materials Research Society, Pittsburgh, 1992), p. 325.
[22] D. P. Brunco, M. O. Thompson, D. E. Hoglung, M. J. Aziz, H.-J. Gossmann, J. Appl. Phys. **78**, 1575 (1995).
[23] S. L. Sobolev, Usp. Fiz. Nauk **5**, 161 (1991) [Sov. Phys. Usp. **34**, 217 (1991)].
[24] D. Jou, J. Casas-Vazquez, and G. Lebon, *Extended Irreversible Thermodynamics*, 2nd ed. (Springer, Berlin, 1996); J. Non-Equilib. Thermodyn. **21**, 103 (1996).
[25] R. E. Nettleton and S. L. Sobolev, J. Non-Equilib. Thermodyn. **20**, 205 (1995); **20**, 297 (1995); **21**, 1 (1996).
[26] D. Jou, J. Camacho, and M. Grmela, Macromolecules **24**, 3597 (1991).
[27] S. L. Sobolev, Phys. Lett. A **163**, 101 (1992).
[28] S. L. Sobolev, Phys. Rev. E **50**, 3255 (1994).